Shear-opposed mixed-convection flow and heat transfer in a narrow, vertical cavity

R. B. Mansour and R. Viskanta
Heat Transfer Laboratory, School of Mechanical Engineering, Purdue University, West Lafayette, IN 47907

A combined experimental and theoretical study has been carried out to investigate mixed-convection heat transfer in a narrow, vertical cavity. The shear force is produced at the left side of a cavity by a belt moving upward that constitutes the sixth wall of the cavity. The left wall of the cavity was cooled and the opposite (right wall) was heated. Hence, the buoyancy force tries to bring the fluid down, and the shear force tends to induce upward fluid flow. The test cell was equipped with two heat exchangers and three thermocouple racks for measuring the temperature distributions at 12 different positions. The temperature field was scanned in the cavity for various flow and temperature boundary conditions. Three- and two-dimensional laminar models were used to analyze the problem theoretically. The experimental measurements were found to be in good agreement with the numerical predictions.

Keywords: mixed-convection; flow and heat transfer; vertical cavity

Introduction

Mixed convection in closed cavities occurs in many industrial and materials-processing situations (Jaluria 1992). For example, such a situation arises in the processing of metals or glass in a temperature-controlled chamber (e.g., a furnace) in which a sheet of material is heated or cooled as it is moved with considerable speed along the production line, creating a combined shear and buoyancy flow. Depending on the Reynolds and Grashof numbers, the interaction of thermal buoyancy (natural convection) and shear forces (forced convection) can produce complex flows of practical interest. In natural environment, for example, wind shear imposed on bodies of water such as lakes, ponds, or estuaries combines with buoyancy to produce mixed convection. In the examples mentioned, simultaneous fluid flow and heat and mass transfer may occur, and little research attention has been devoted to these types of transport problems.

The natural-convection problem in an enclosed cavity has been studied numerically and experimentally. A comprehensive study has been reported by Henkes (1990) for a differentially heated cavity. The problem of lid-driven cavities with or without heat transfer has received considerable attention in numerous numerical studies published during the last two decades (Mohamad 1992). In addition to its industrial relevance, the problem has also served as a benchmark flow model to test various computational schemes (Iwatsu et al. 1989).

Unlike natural convection, only a few experimental studies have been published for the shear-driven cavity flows. The major works are by Grand (1975), Koseff and Street (1984), and Mohamad and Viskanta (1990). In the cited studies, flow visualization and velocity measurements have been performed with water and glycerine. Also, temperature distribution measurements were made in water, glycerine, and liquid gallium.

The authors are not aware of any experimental studies with air as the working fluid in which temperature measurements have been made in combined shear-buoyancy-driven cavity flows. These types of physical situations present some experimental difficulties in making accurate flow visualizations in a closed air-filled cavity with a moving wall. For the present study, temperatures are measured in an air-filled cavity in which the vertical left wall moves with a constant speed. Air is the working fluid in coating, anodizing, and other industrial applications; therefore, it is of considerable interest to experiment directly with air, rather than to replace it with a fluid that is easier to handle.

Experimental apparatus and test procedure

The purpose of the experiments was to simulate mixed convection in an air-filled cavity produced by thermal buoyancy and shear forces imposed by the motion of the left-side wall. Air was chosen as a fluid because of its relevance to materials-processing applications, which typically involve combustion products or other gases. The physical situation considered may simulate, for example, a heat-treating oven in which a sheet of material (i.e., metal) may be moved vertically in the chamber. Depending on the speed of the material and the dimensions of the chamber, the Reynolds number may vary over a wide range, and the flow could be in laminar, transition, or turbulent flow regimes. The main objective in this study was to measure the temperature distributions and to deduce the flow structure in as many locations as possible in order to gain an understanding of the effects of side surface motion (shear) on the heat transfer.

Address reprint requests to Professor Viskanta at the Heat Transfer Laboratory, School of Mechanical Engineering, Purdue University, West Lafayette, IN 47907-1288, USA.

Received 3 February 1994; accepted 11 July 1994

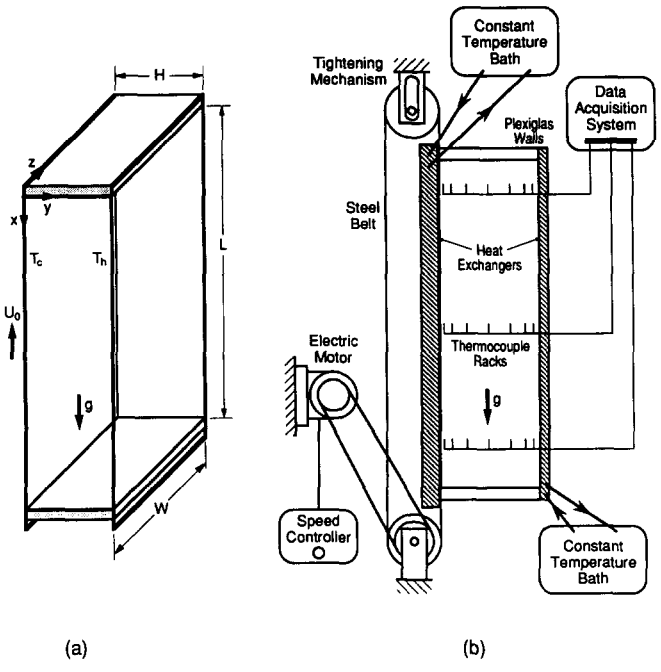

Figure 1 Schematic of the experimental setup (a) and physical model (b) for the vertical tall cavity

A schematic diagram of the apparatus is shown in Figure 1. The main parts of the experimental set-up are the five-wall cavity, the moving belt (sixth wall), the heat exchangers, and an electric motor driving the belt. The test cell is made of four walls cut of acrylic (Plexiglas). The walls are glued together and bolted to the right heat exchanger. The dimensions of the test cell are $10 \times 5 \times 30$ cm. These dimensions were chosen to obtain an aspect ratios of $6 \times 2 \times 1$. Preliminary numerical calculations for this model have shown that an aspect ratio of five or greater simulates well the narrow cavity. The transverse aspect ratio of two was selected based on preliminary numerical calculations that revealed the three-dimensional (3-D) nature of the flow structure with symmetry. The left, moving side wall of the test cell is made of a stainless steel belt that was specially welded to minimize the seam size. The belt slides on the second (left) heat exchanger. The belt has a tightening mechanism that acts with the heat-exchanger support and ensures that the belt is in direct contact with a plane surface. A clearance of less than 1 mm is left between the five walls and the belt to ensure smooth running of the belt and to reduce the vibration of the system to a minimum. This clearance is essential even though it may cause air entrainment.

Experiments were initiated by heating/cooling the heat exchangers to the desired hot and cold temperatures. This was done with the aid of two constant-temperature baths. The temperatures of both heat exchangers were monitored by six thermocouples (three in each) that were embedded in the vicinity of the control surfaces.

Once the left and right walls have reached steady and uniform temperatures, the data collection is started for time analysis. It takes one to two hours to reach steady or quasi-steady conditions for thermal buoyancy driven flow in the cavity. When the belt motion is activated, the time to achieve steady state is reduced to 30 minutes or less.

The 27 thermocouples are connected to a Hewlett Packard data acquisition system (9800 model series) that is capable of processing all the channels in under 10 seconds. The signals are processed, printed on a terminal screen, and stored on a computer disk for further analysis.

A wire-smoke method was attempted to obtain qualitative flow structure information; however, the method was not very successful because of some smoke accumulation and mixing in the cavity. Heat transfer measurements at the moving wall (belt) would have been highly desirable, but sophisticated methods needed to be developed and employed that were beyond the scope of the present work.

The experiments were performed for three different belt speeds, in addition to the stationary-left-side (i.e., zero-speed) case. The belt motion is in the upward direction for all the experiments. The other system parameter is the temperature difference between the heat exchangers. The experiments could be repeated under the same conditions to collect temperature data in as many positions as possible. Three thermocouple racks capable of rotating around their axes (see Figure 1) provided the opportunity to collect temperature data at each angular position. Only the four right-angle positions were exercised. The spanwise positions allow validation of 3-D numerical models. In total, more than 16 sets of experiments

Notation

A	Aspect ratio, L/H
c_p	Specific heat at constant pressure (J/kg · K)
Gr	Grashof numbers, $g\beta\Delta TH^3/\nu^2$
H	Cavity width (m); see Figure 1
k	Thermal conductivity
L	Cavity height (m); see Figure 1
P, p	Dimensionless or dimensional pressure (Pa)
Pr	Prandtl number, $\mu c_p/k$
Re	Reynolds number, $\rho U_0 H/\mu$
Ri	Richardson number, Gr/Re^2
T	Temperature (K)
T_c	Cold-wall temperature (K)
T_h	Hot-wall temperature (K)
t	Time (s)
U, u	Velocity component in the X-(x-) direction (m/s)
U_0	Bottom velocity (m/s)
V, v	Velocity component in the Y-(y-) direction (m/s)
W, w	Velocity component in the Z-(z-) direction
X, x	Coordinate defined in Figure 1b
Y, y	Coordinate defined in Figure 1b
Z, z	Coordinate defined in Figure 1b

Greek symbols

ε	Turbulent kinetic-energy dissipation (m^2/s^3)
μ	Dynamic viscosity ($N \cdot s/m^2$)
ν	Kinetic viscosity (m^2/s)
ρ	Density (kg/m^3)
Θ	Dimensionless temperature, $(T - T_c)/(T_h - T_c)$

Subscripts

H	Based on cavity width H as characteristic length
L	Based on cavity height L as characteristic length

Superscripts

$'$	Fluctuating component
-	Averaged quantities

were performed. Only a few of these are presented in the results sections.

Analysis

At moderate Rayleigh numbers ($2 \times 10^3 < \mathrm{Ra} < 1 \times 10^7$), the flow in a differentially heated cavity is laminar (Henkes 1990). To simulate the experiments performed, a mathematical model has been developed. The physical model and coordinate system are shown in Figure 1.

We start from the 3-D conservation equations and assume the following:

(1) the fluid is Newtonian, incompressible, and the flow is laminar and steady;
(2) viscous heat dissipation is negligible in comparison with conduction and convection;
(3) all thermophysical properties are constant except the density, and its variation with temperature is accounted for only in the buoyancy term using the Boussinesq approximation; and
(4) radiation is negligible in comparison to convection.

In order to reduce the number of independent variables and to identify relevant scaling parameters, the model equations are first nondimensionalized. We introduce the relevant dimensionless variables defined in the nomenclature and choose the short side of the cavity, H, as the characteristic length scale, since it has been found to be the appropriate scale for shallow cavity flows (Mansour 1993). The spacing H may not be the appropriate scale for natural convection in a narrow vertical cavity. However, the spacing H was chosen as the relevant length scale for buoyancy and shear-driven mixed-convection flows in both horizontal and vertical shallow cavities (the short side is parallel or normal to the gravity vector, respectively). The dimensionless conservation equations of mass, momentum, and energy can be written as

$$\nabla \cdot \vec{V} = 0 \tag{1}$$

$$(\vec{V} \cdot \nabla \vec{V}) = (1/\mathrm{Re})\nabla^2 \vec{V} - \nabla P + (\mathrm{Gr}/\mathrm{Re}^2)\vec{k}\Theta \tag{2}$$

and

$$\vec{V} \cdot \nabla \Theta = (1/\mathrm{Re\ Pr})\nabla^2 \Theta \tag{3}$$

respectively.

The velocity boundary conditions are

$$U = U_0 = -1,\ V = W = 0 \quad \text{at} \quad Y = 0 \quad \text{and} \quad 0 < X < A \tag{4}$$

$$U = V = W = 0 \quad \text{at} \quad Y = 1 \quad \text{and} \quad 0 < X < A \tag{5}$$

At all remaining boundaries, the no-slip boundary conditions were imposed. With the cavity heated from the left side, the temperature boundary conditions are

$$\Theta = 0 \quad \text{at} \quad Y = 0 \quad \text{and} \quad 0 < X < A \tag{6}$$

$$\Theta = 1 \quad \text{at} \quad Y = 1 \quad \text{and} \quad 0 < X < A \tag{7}$$

All remaining boundaries were assumed to be adiabatic (insulated).

Numerical results are reported in this paper for three different models: (1) 3-D laminar flow (3DL), (2) two-dimensional (2-D) laminar flow (2DL), and (3) 2-D turbulent flow (2DT). The k–ε turbulence model is described elsewhere (Mansour and Viskanta 1992) and need not be repeated here. The 2-D model results are included for the purpose of comparison with the 3DL results to assess under what conditions 2DL and 2DT model predictions may be adequate.

The numerical method employed to solve the transport equations is the widely used SIMPLER scheme (Patankar 1980). Details of the method are well described in computational literature and need not to be repeated here.

The 2DL and 2DT models have been extensively tested by comparing the numerical predictions with published experimental data of previous investigators such as Grand (1975) and Cheesewright et al. (1986). To validate the model further, an extensive grid-independence study was performed, and computational details are available elsewhere (Mansour 1993). A sinusoidal (sin) grid with 61×31, 81×31, and 101×41 were tested. A sinusoidal (sin) grid distribution is used for the laminar model and a sinusoidal squared ($\sin^2$) grid is employed for the turbulent model in order to capture the viscous sublayer with a minimum number of grid points. The 2DL model results reported in this paper were generated using a sinusoidal grid of 81×31 in the x- and y-directions, respectively, and the 3DL model predictions were made using a grid of $61 \times 31 \times 21$.

Results and discussion

Experimental temperature profiles

The experiments discussed in this paper are summarized in Table 1. The range of the Reynolds number in combination of the Grashof number allowed the Richardson number ($\mathrm{Ri}_H = \mathrm{Gr}_H/\mathrm{Re}_H^2$ to vary between 0.1814 to 4.704, which is sufficient for a study of the interaction between the buoyancy and shear forces. To obtain higher Reynolds number, a more sophisticated experiment needs to be designed to minimize vibration due to the belt motion and reduce entrainment of outside air into the test cavity.

The temperature histograms for Experiments 31 ($\mathrm{Re}_H = 257$) and 33 ($\mathrm{Re}_H = 934$), both of which are for $\mathrm{Gr} = 1.58 \times 10^5$, are reported ($X = 3.36$) in Figure 2. Overall, the temperature signals characterize a stable, steady-state behavior, except for

Table 1 Summary of experiments with heating of the right wall (the dimensionless parameters are based on the distance H as a characteristic dimension)

Run	T_c (K)	T_h (K)	ΔT (K)	u_{belt} (m/s)	$\mathrm{Re}_H \times 10^2$	$\mathrm{Gr}_H \times 10^5$	Ri_H
10	25.0	45.0	20.00	0	0	2.94	0
11	25.0	45.0	20.00	0.083	2.50	2.94	4.70
12	25.0	45.0	20.00	0.210	6.31	2.94	0.739
13	25.0	45.0	20.00	0.302	9.08	2.94	0.357
30	25.0	35.0	10.00	0	0	1.58	0
31	25.0	35.0	10.00	0.083	2.57	1.58	2.39
32	25.0	35.0	10.00	0.210	6.49	1.58	0.376
33	25.0	35.0	10.00	0.302	9.34	1.58	0.181

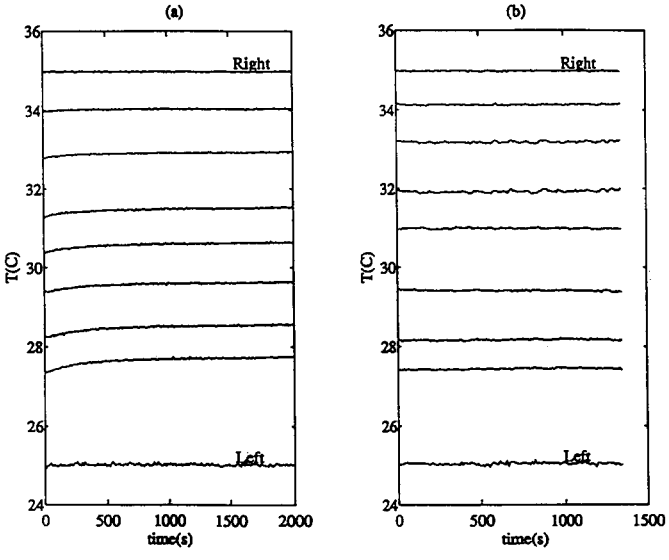

Figure 2 Temperature histograms of Experiment 31 (a) and Experiment 33 (b) for the middle-rack thermocouples ($X = 3.36$)

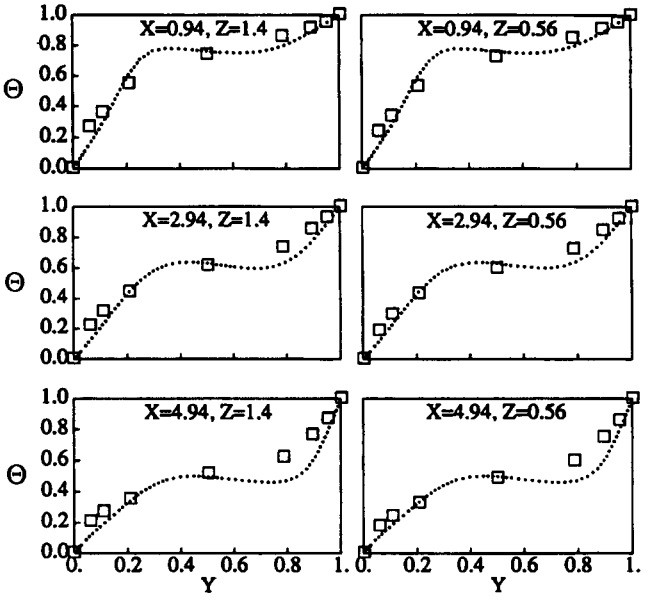

Figure 3 Comparison of measured and predicted (using 3DL model) temperature profiles at lateral positions for Experiment 32. In the figure, the symbols denote data and the dotted line denotes predictions based on the 3DL model

a few fluctuations smaller than 0.1°C that are mostly due to unsteadiness in the heat-exchanger temperatures. The steadiness of the temperature signals, including Fast Fourier Transform (FFT) analysis results (Mansour 1993), implies that the flow should be laminar, and hence the 2DL and 3DL models should result in better predictions than the 2DT model. This is indeed the case for most measured locations, as can be seen in Figures 3 and 4, where the predicted and measured temperatures are compared for Experiment 32. The agreement between the predictions based on the laminar flow model and the data is very good in the center X–Y plane (Figure 4) and for the lateral positions (Figure 3), with the exception of a few locations in the bottom part of the cavity ($X > 4.5$ and $0.7 < Y < 0.9$). These exceptions may be due to a large conduction error in temperature readings, since the velocities in that region are small, as the predicted flow field will show. A similar conclusion can be drawn from additional comparisons for Experiment 13, reported elsewhere (Mansour 1993) for a higher Grashof number. This conclusion suggests that even for $Re_H = 908$ and $Ri_H = 0.357$, the flow is still laminar.

Prediction of flow and temperature fields

The interaction between the shear and buoyancy forces is such that interesting flow behavior may develop. Starting with Experiment 31 ($Gr = 1.58 \times 10^5$, $Re = 257$), in which the buoyancy force dominates the flow as shown in Figure 5, the shear cell occupies a very small extent of the cavity. The extent of the cell is large at the upper and lower left corners, since the shear overcomes the buoyancy in those parts of the cavity. As the shear speed is increased, the extent of the cell grows. It occupies about 20 percent of the space when $Re_H = 649$ (Experiment 32) (Mansour 1993) and 30 percent of the cavity when $Re_H = 934$ (Experiment 33) as shown in Figure 6. In the upper left corner, the shear cell penetrates half the cavity width (Figure 6) as the sheared flow is forced to take a 90° turn at the upper end wall and extends the inertia-driven flow up to the point where the buoyancy cell takes over. The 2DT model predictions of Experiment 33 are also presented in Figure 7. The flow and temperature fields are similar to the laminar predictions, but the 2DT model predicts a larger shear cell.

At the interface between the cells, the velocity gradients are equal and opposite, creating equal shear forces and zero velocity. As a result of this interaction, the cavity is divided into two almost independent regions, in one of these, the flow is mainly driven by inertia, and in the other, the flow is completely driven by buoyancy. Given two different fluids in which the flow is characterized by such behavior, little advective mixing would be expected. For example, if one fluid carries a pollutant, it can penetrate the other unpolluted fluid stream only through mass diffusion. At the interface, we can

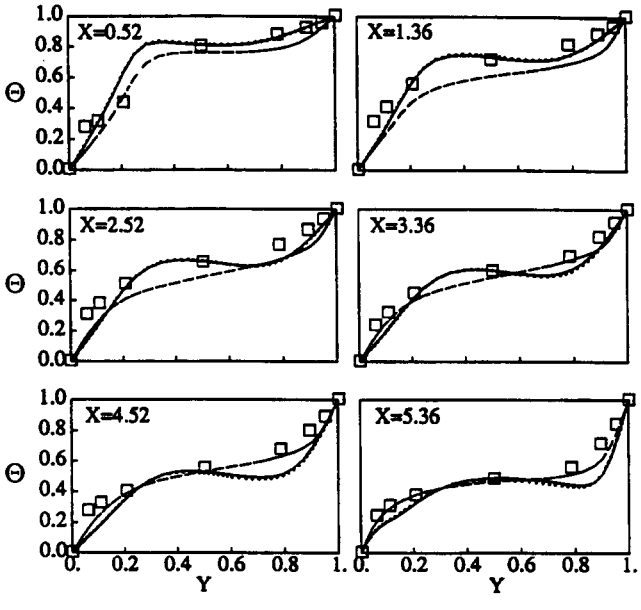

Figure 4 Comparison of measured and predicted (using 3DL model) temperature profiles at symmetry plane for Experiment 32. Numerical predictions are indicated as follows: □, experimental; ——, 2DL; ..., 3DL; ———, 2DT

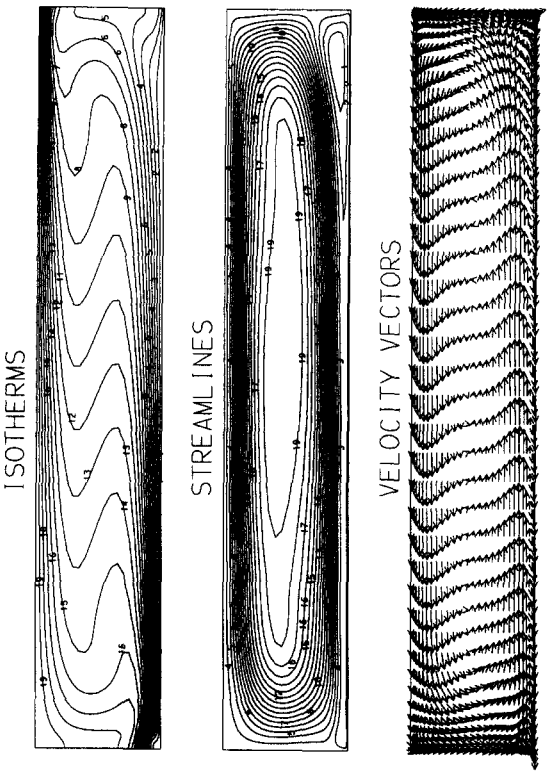

Figure 5 Two-dimensional transport fields, predicted using the 2DL model for Experiment 31. Refer to Figure 1a for coordinates

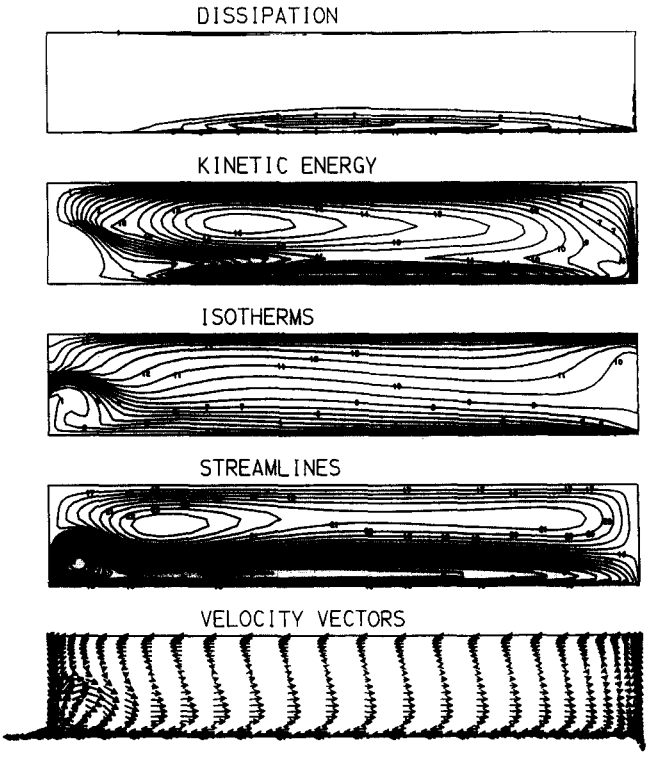

Figure 7 Two-dimensional transport fields, predicted using the 2DT model for Experiment 33. Refer to Figure 1a for coordinates

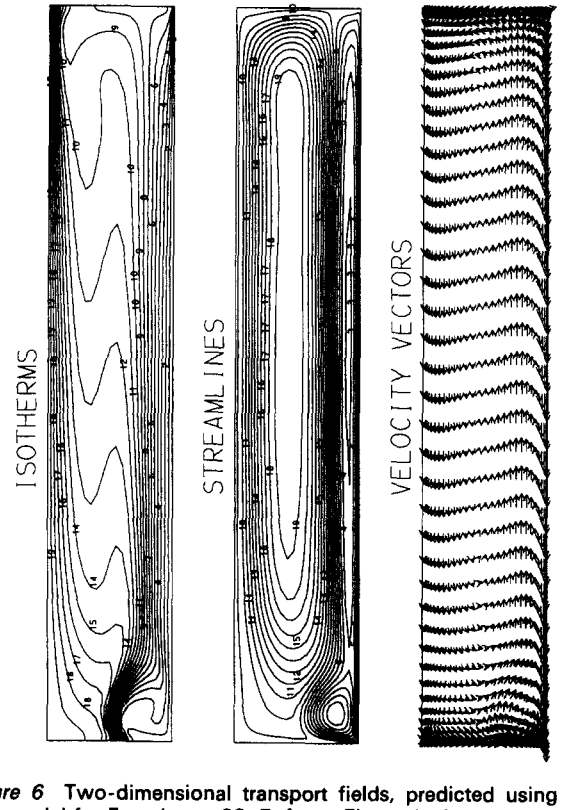

Figure 6 Two-dimensional transport fields, predicted using the 2DL model for Experiment 33. Refer to Figure 1a for coordinates

also observe that the temperature profiles are linear (Figures 3 and 4).

The 3DL model was exercised to simulate the 3-D flow (Figure 8) and temperature (Figure 9) fields for Experiment 32. Some U–V and U–W velocity vector plots in the X–Y and Z–Z planes are shown in Figures 8a and 8b, respectively. The V–W velocity vectors do not reveal any new flow-structure information beyond that shown and are, therefore, not included for the sake of brevity. The velocity vector plots show that, in the major part of the cavity, the flow is nearly 2-D and the 3-D effects are confined to the regions near the lateral side walls (i.e., $Z \sim 0$ and $Z \sim 2.0$) and ends of the cavity. The U–V velocity vector plots reveal that the shear cell is smaller near the side walls and largest near the center plane ($Z = 1.0$). The effects of the lateral side (at $Z = 0$ and $Z = 2.0$) and end walls (at $X = 0$ and $X = 5.88$) are also evident and are revealed by small corner flow cells.

The isotherms in selected X–Y, X–Z, and Z–Y planes are plotted in Figures 9a, 9b, and 9c, respectively. The panels of Figure 9b reveal that the temperature distribution is symmetric about the middle plane ($X = 1.0$). In addition, the different panels of Figure 9a show that the temperature gradients are largest near the cold ($Y = 0$) and hot ($Y = 1.0$) walls, with the core of the flow ($0.3 \sim Y \sim 0.7$) being rather uniform in temperature. The panels of Figures 9a and 9c clearly show the regions of flow where the isotherms are the densest and the local convective heat fluxes the highest.

It was determined from temperature measurements as well as flow and thermal structures predictions that the flow is 2-D only up to $\mathrm{Re}_H < 800$ and $\mathrm{Gr}_H < 2 \times 10^5$. In this range of parameters, the 2DL, 2DT, and 3DL model predictions were in good agreement with each other, and the 3DL model yielded a physically acceptable solution. Beyond this range of parameters, the 3DL model could not converge. In addition,

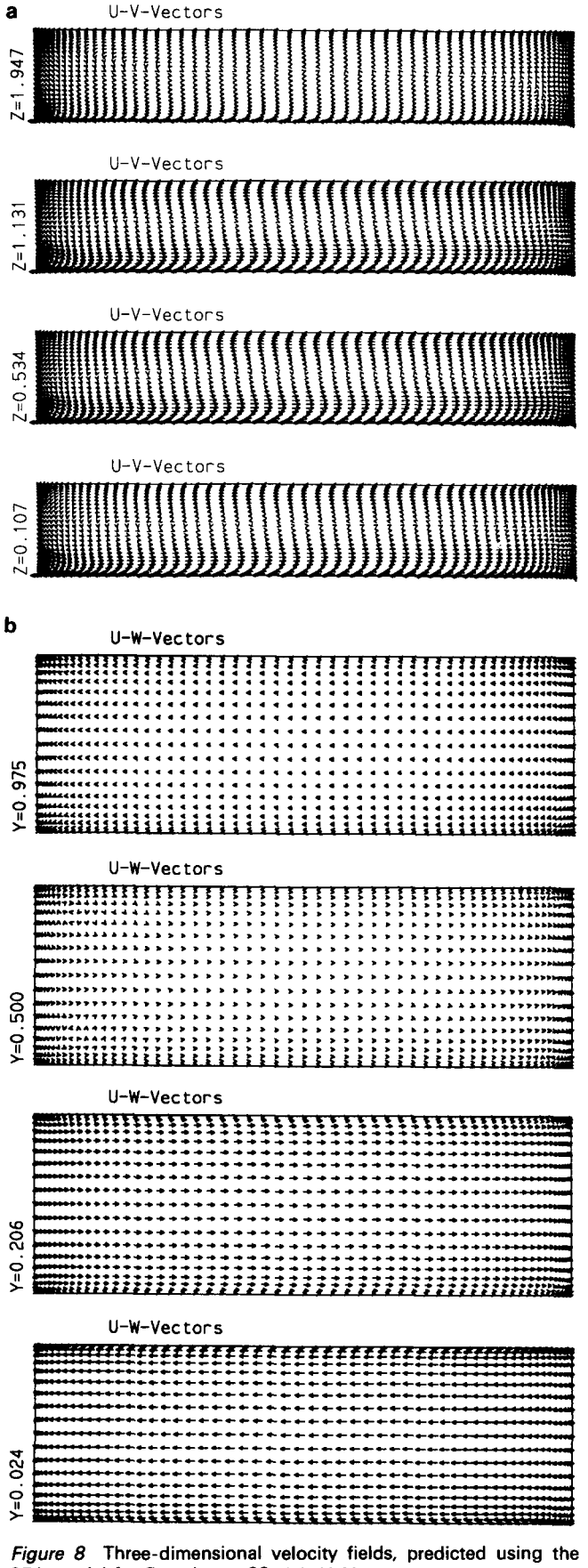

Figure 8 Three-dimensional velocity fields, predicted using the 3DL model for Experiment 32. (a) *U–V* vectors in the *X–Z* plane; (b) *U–W* vectors in the *X–Z* plane. Refer to Figure 1a for coordinates

the 2DL and 2DT the model predictions started to differ. Hence, it is most probable that the flow became 3-D, as has been shown in experimental (Koseff and Street 1984) and numerical (Iwatsu et al. 1989) studies. It is interesting to note that for the shear-opposed buoyancy-aided flow, the transition to turbulence flow is delayed, while in shear-assisted buoyancy-aided flow, the transition to turbulence is advanced (Mansour 1993).

Prediction of heat transfer

The local heat transfer rate is directly affected by the flow separation. The local Nu distribution is given for Experiment 32 in Figure 10. At the left wall, the 2DL and 3DL results practically coincide with each other, and the local Nusselt numbers predicted by the 2DT model are somewhat higher. At the right wall, the 2DL and 3DL are also very close, and the 2DT results differ somewhat, particularly at the bottom and top of the wall. The results for Experiment 33 are very similar and are not given here for the sake of brevity but can be found elsewhere (Mansour 1993). The distribution at the left wall is strongly affected by the shear cell, and the distribution at the right wall is uniquely formed by the natural-convection cell. The 2-D Nu distributions computed from the 3DL model simulation for Experiment 32 are shown in Figure 11. The 3DL model predictions are very close to those of the 2DL model. The local Nusselt number distributions at both the right wall (Figure 11a) and at the left wall (Figure 11b) are practically independent of the spanwise coordinate Z, except for the endwalls and corners, where the flow is strongly 3-D. We also note that, in this case, the Nusselt number does not decrease monotonically, but rather a local maximum is formed near the upper-left corner of the cavity. Examination of the flow and temperature fields reveals that the shear cell in the present simulation is confined to a smaller space that pushes the isotherms closer together, producing a higher heat transfer rate at that location.

The overall effect of the shear–buoyancy interaction on the heat transfer rate can be deduced from the average Nusselt number $\overline{\mathrm{Nu}}$. Table 2 summarizes all experiments that have been simulated. Starting from the base case value of $\overline{\mathrm{Nu}} = 3.685$, for the natural-convection Experiment 30, $\overline{\mathrm{Nu}}$ is reduced to 3.048 as shear is introduced ($\mathrm{Re}_H = 250$). $\overline{\mathrm{Nu}}$ keeps on decreasing until a critical Richardson number Ri* is reached at which $\overline{\mathrm{Nu}}$ has attained an absolute minimum. Increasing Re_H beyond this point increases $\overline{\mathrm{Nu}}$. The same trend is observed for Experiments 11, 12, and 13.

Normally, the critical Richardson number, Ri*, is expected to be of the order of unity if the parameters are scaled properly. Basing Ri on H, the cavity width, does not bring Ri* close unity. On the other hand, if one is to base Ri on L, the height of the vertical cavity, the predicted Ri* would be very close to, though not exactly, unity. Hence, the mathematical-model results support the supposition that Ri_L, Re_L, and Gr_L are more appropriate than Ri_H, Re_H, and Gr_H, as was deduced from the scaling analysis (Mansour 1993); however, this conclusion should be tempered, since additional experimental data and predictions are needed to confirm this assertion.

In order to further verify the trends predicted for the interaction of the shear and buoyancy forces and their effect on heat transfer, a systematic study was conducted to extend the range of independent parameters well beyond those that could be achieved experimentally. The 2DT model was used, and the results of the calculations performed at higher Grashof and Reynolds numbers are presented in Table 3. The results show that there is a minimum in the average Nusselt number $\overline{\mathrm{Nu}}$ with the Richardson number Ri_H (or Ri_L) for $\mathrm{Gr}_H = 1 \times 10^6$,

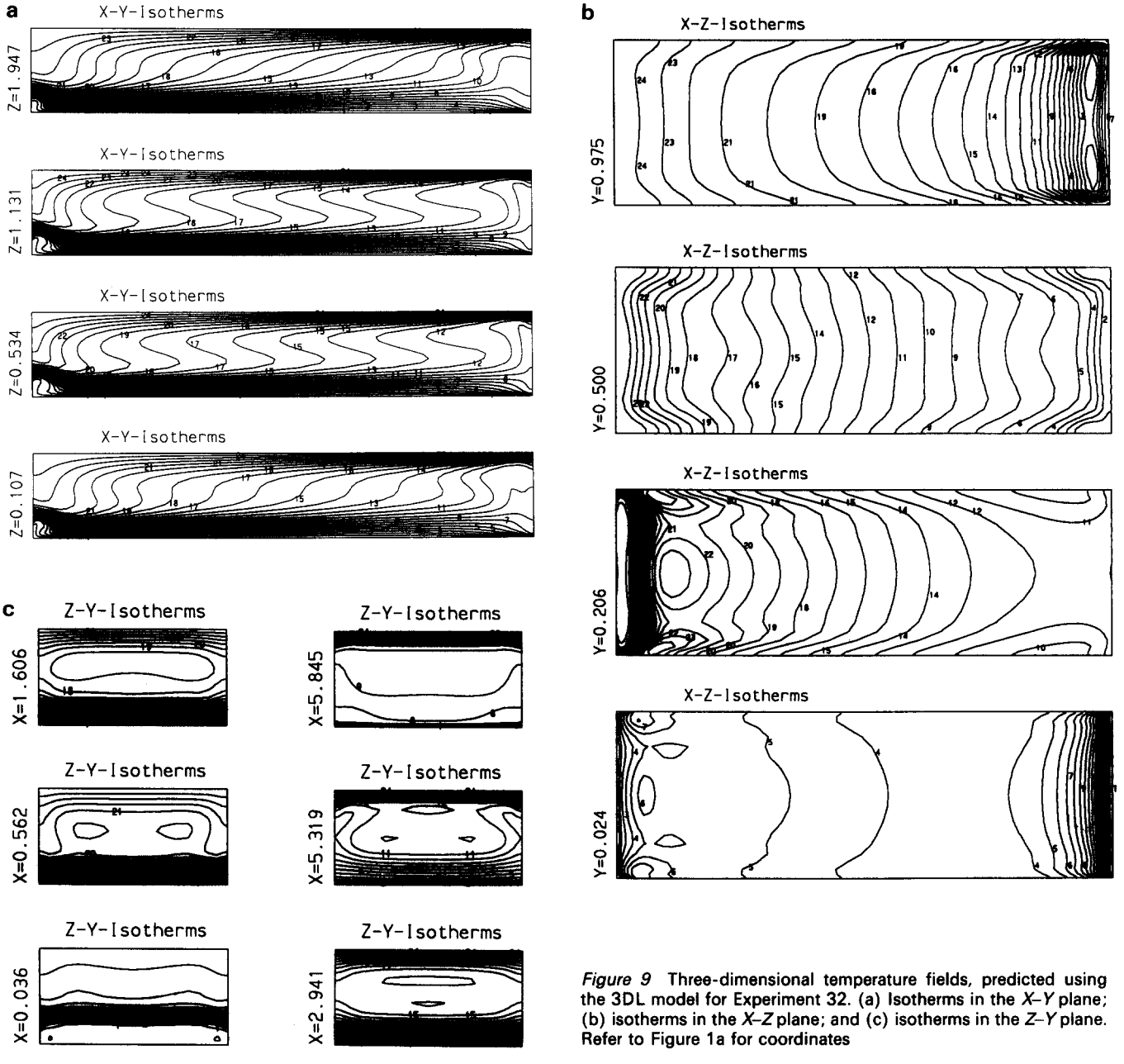

Figure 9 Three-dimensional temperature fields, predicted using the 3DL model for Experiment 32. (a) Isotherms in the *X–Y* plane; (b) isotherms in the *X–Z* plane; and (c) isotherms in the *Z–Y* plane. Refer to Figure 1a for coordinates

1×10^7, and 1×10^8. The results presented are consistent with those reported elsewhere for shear-aided mixed-convection flow and heat transfer in narrow, vertical cavities (Mansour 1993).

Heat transfer data at the moving wall (belt) would have been very desirable. Unfortunately, entrainment of ambient air into the cavity by the moving belt and experimental difficulties in measuring local surface temperatures and heat fluxes with acceptable uncertainty precluded making these measurements.

Conclusions

Experimental measurements and predictions are reported for combined shear-opposed buoyancy-driven flow in a narrow, vertical cavity filled with air.

(1) The numerical simulations have revealed that the shear force can alter the flow structure by reducing the extent of

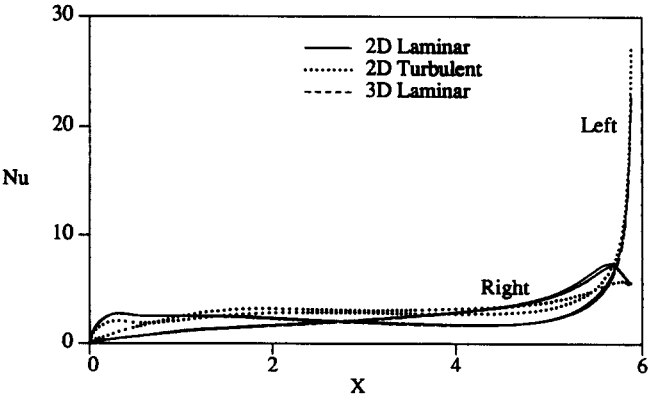

Figure 10 Local Nu distribution, predicted by the 2DL, 3DL, and 2DT models for Experiment 32

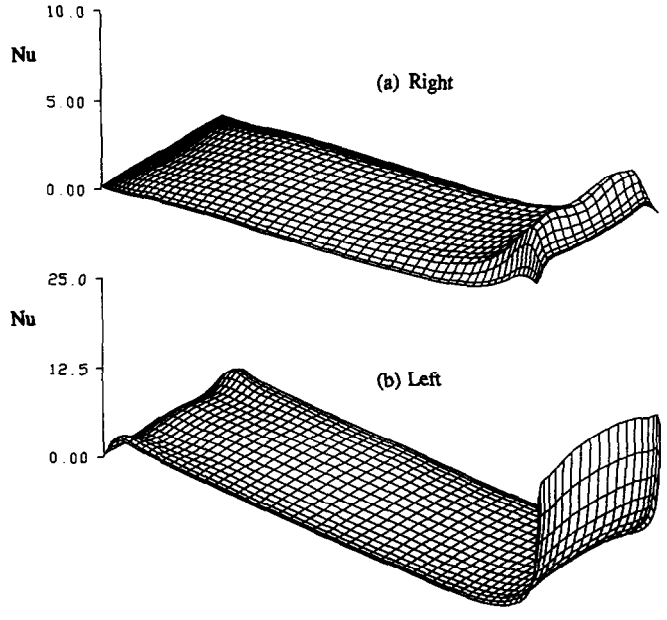

Figure 11 Two-dimensional Nu distributions, predicted using the 3DL model at the right (a) and the left (b) walls of the cavity for Experiment 32

Table 2 Predicted average Nusselt numbers ($\overline{Nu}$) for shear-opposing-buoyancy mixed convection for the experimental conditions

		Re_H					
Model	$Gr_H \times 10^{-5}$	0	250	710	920	1316	4160
2DL	1.58	3.68	3.05	2.63	2.68		
3DL	1.58	3.58		2.55			
2DT	1.58	4.11		3.13	3.37		
2DL	2.94	4.28	3.73	3.19	3.06	3.17	6.60
2DT	2.94				3.89	4.22	11.1

the stagnant core and changing the thickness of the boundary layers. The Richardson number is still the controlling parameter, and when $Ri_H < 1$, the shear controls the flow and heat transfer inside the narrow vertical cavity. In the presence of shear, the convective heat transfer rate is enhanced, but the local distributions again strongly depend on the Richardson number.

(2) When the cavity is driven simultaneously by buoyancy and shear forces that oppose each other, an interesting flow structure develops. A shear cell develops adjacent to the moving boundary, while the buoyancy cell fills the rest of the cavity. The respective size of each cell depends on the Richardson number.

(3) When shear opposes buoyancy, the heat transfer rate is reduced below that for natural convection. The rate continues to decrease until a minimum is reached at around $Ri_L = 1$. Further increase of shear velocity increases the heat transfer rate as the flow becomes dominated by the shear force.

(4) Through the numerous simulations made for the vertical arrangement, the mathematical model has established that the correct scaling length for mixed convection inside the narrow cavity is the cavity height L rather than its width H. This is in agreement with the findings of the order-of-magnitude analysis, but experimental data and more extensive numerical results are needed to confirm this assertion.

(5) The results obtained indicate that a 3-D model capable of simulating turbulent flow and heat transfer is needed to predict transport in cavities with higher Reynolds and Grashof numbers. Also, experiments need to be performed under conditions more prototypic of industrial applications to obtain data required for model validation.

Table 3 Average numbers ($\overline{Nu}$) for shear-opposing-buoyancy mixed convection at high Gr and Re numbers with $A = 5.88$

Gr_H	Re_H	Ri_H	Ri_L	$\overline{Nu}$
	0	∞	∞	7.68
1×10^6	1,000	1	5.88	6.08
	5,000	0.04	0.235	11.82
	10,000	0.01	0.0588	21.98
	0	∞	∞	14.53
1×10^7	1,000	10	58.8	14.06
	5,000	0.4	2.35	14.34
	10,000	0.1	0.588	19.96
	0	∞	∞	35.73
	1,000	100	588	28.53
1×10^8	5,000	4	23.52	24.56
	10,000	1	5.88	26.20
	20,000	0.25	1.47	37.45
	50,000	0.04	0.235	74.35

References

Cheesewright, R., King, K. J., and Ziai, S. 1986. Experimental data for the validation of computer codes for the prediction of two-dimensional buoyant cavity flows. In *Significant Questions in Buoyancy Affected Enclosure or Cavity Flows*, J. A. C. Humphrey, C. T. Avedisian, B. W. Le Tourneau, and M. M. Chen (eds.). ASME, New York, 75–81

Grand, D. 1975. Contribution à l'étude des courants de recirculation. These du Doctorat d'Etat en Sciences Physiques, Université Scientifique et Médicale et Institut Nationale Polytechnique, Grenoble

Henkes, R. A. W. M. 1990. Natural convection boundary layers. Ph.D. thesis, Delft University of Technology, The Netherlands

Iwatsu, R., Ishii, K., Kawamura, T., Kuwahara, K., and Hyun, J. M. 1989. Numerical simulation of three-dimensional flow structure in a driven cavity. *Fluid Dynam. Res.*, **5**, 173–189

Jaluria, Y. 1992. Transport from continuously moving materials undergoing thermal processing. In *Annual Review of Heat Transfer*, Vol. 4, C. L. Tien (ed.). Hemisphere, Washington, 187–245

Koseff, J. R. and Street, R. L. 1984. The lid-driven cavity flow: a synthesis of qualitative and quantitative observations. *J. Fluids Eng.*, **106**, 390–398

Mansour, R. B. 1993. Radiative and convective heat transfer in shear driven cavities. Ph.D. thesis, Purdue University, West Lafayette, IN

Mansour, R. B. and Viskanta, R. 1992. Fluid flow and heat transfer in shallow cavities driven by shear and buoyancy. In *Fundamentals of Mixed Convection*, HTD-Vol. 213, T. S. Chen and T. Y. Chu (eds.). ASME, New York, 31–42

Mohamad, A. A. 1992. Mixed convection in lid-driven cavities. Ph.D. thesis, Purdue University, West Lafayette, IN

Mohamad, A. A. and Viskanta, R. 1990. Combined surface shear and buoyancy-driven convection in a shallow cavity. In *Fundamentals of Natural Convection*, HTD-Vol. 140, V. S. Arpaci and Y. Bayazitoglu (eds.). ASME, New York, 1–7

Patankar, S. 1980. *Numerical Heat Transfer and Fluid Flow*. Hemisphere, McGraw-Hill, Washington